Proc. Natl. Acad. Sci. USA
Vol. 86, pp. 1870–1874, March 1989
Cell Biology

Quantitative imaging of free and total intracellular calcium in cultured cells

(fura-2/ion microscopy/secondary ion mass spectrometry/NIH 3T3 cell line/L6 myoblast cell line)

SUBHASH CHANDRA*, DAVID GROSS†‡, YONG-CHIEN LING*, AND GEORGE H. MORRISON*

*Department of Chemistry and †School of Applied and Engineering Physics, Cornell University, Ithaca, NY 14853

Communicated by Robert H. Wasserman, November 28, 1988 (received for review May 23, 1988)

ABSTRACT **Techniques of fluorescence and ion microscopies were combined to study the free [Ca^{2+}] and total Ca in NIH 3T3 fibroblast and L6 rat myoblast cells. Free Ca^{2+} measurements with the Ca^{2+} indicator fura-2 and digital imaging reveal an inhomogeneous distribution of free cytoplasmic Ca^{2+} in both cell lines. Fura-2 also reveals a difference in free Ca^{2+} activity between the nucleus and cytoplasm of cells. Ion microscopic observations on sister cells show that total Ca in the cytoplasm is also inhomogeneously distributed and that mean cytoplasmic levels of total Ca are higher than levels in the nuclei. In the nuclei of NIH 3T3 cells, the mean free [Ca^{2+}] and total [Ca] were 110 ± 30 nM and 225 ± 43 μM, respectively, while regions in the cell cytoplasm contained up to 490 ± 270 nM free [Ca^{2+}] and 559 ± 184 μM mean total [Ca]. Intracellular total Ca was >3 orders of magnitude higher than intracellular free Ca^{2+} in either nuclear or cytoplasmic compartments. Perinuclear cytoplasmic regions in 3T3 cells contained higher free and total Ca than the cell nucleus. Loading of cells with fura-2 did not modify the subcellular distribution of total K, Na, Ca, or Mg. This combination of two powerful ion imaging techniques provides a comparison between free and total calcium in cells and introduces a different approach for examining the role of this important element in cell physiology.**

The movement and storage of calcium has long been recognized as a critical regulatory mechanism of cell activity. Phenomena as diverse as muscle contraction and stimulus-secretion coupling are accompanied by dramatic changes in intracellular free Ca^{2+} levels. Ca^{2+} has often been implicated as a mediating messenger in the transduction of cell signals. Measurements of the subcellular distribution of Ca^{2+} are needed to study localized cytoplasmic fluxes and sequestration of calcium to understand and evaluate the role of this important ion in physiological events. However, such measurements pose one of the most challenging problems in cell biology. We combined fluorescence microscopy using the Ca^{2+} indicator fura-2 (1) and the technique of ion microscopy (2–4) to study, respectively, the subcellular distribution of free Ca^{2+} and total (both free and bound) Ca in unsynchronized NIH 3T3 mouse fibroblast and L6 rat myoblast cells. Our observations demonstrate that the subcellular distribution of both free and total Ca are spatially heterogeneous within these cells and that the free Ca^{2+} and total Ca distributions have some intriguing similarities and differences.

MATERIALS AND METHODS

Combining Fluorescence and Ion Microscopy. Combining these two entirely different techniques required the modification of sample preparation procedures of each technique to accommodate the needs of the other. Subcellular free Ca^{2+} measurements using fura-2 are made on live cells, while the measurements for total Ca with ion microscopy must be made on fixed cells grown on electrically conducting substrate since the cell sample is biased at 4500 V in the high vacuum chamber (≈10^{-8} torr; 1 torr = 133.3 Pa) of the ion microscope. Semiconductor grade silicon wafer pieces (≈1 cm^2) polished to submicron flatness serve well as a cell growth substrate for measurements by ion microscopy. This substrate is nontoxic and allows comparable cell growth rates and morphology as compared to cells grown on glass coverslips. In addition, cells cultured on silicon can also be examined by fluorescence microscopy, as demonstrated by previous DNA staining work (5). Quenching of fluorescence for fluorphores near a conducting silicon surface occurs efficiently over distances of ≈50 nm (6). Thus, quenching of cytoplasmic fura-2 fluorescence by this mechanism is negligible.

After the free cytoplasmic Ca^{2+} distributions within several cells were measured with fura-2 by fluorescence microscopy, cells on the same silicon wafer or on another bearing sister cells maintained under identical conditions were processed for ion microscopic measurements. At this stage in the procedure, the cells were fixed in their native state for ion microscopic analysis. However, the extracellular fluid, which is essential for maintaining the cells during fura-2 measurements, had to be eliminated to analyze cells without contamination. Any attempt to wash away the extracellular fluid was suspect as potentially artifactual (7, 8). This obstacle was avoided by using a sandwich-freeze-fracture freeze-drying methodology recently developed in our laboratory (5). In this methodology, the freeze-fracture process produces a few randomly scattered areas containing up to hundreds of cells grouped together where the fracture plane has passed through the apical side of the cell monolayer, leaving the half-membranes and the extracellular fluid on the other (nonsubstrate) side of the sandwich. These apical side fractured cells allow a direct ion microscopic analysis of total Ca, Mg, Na, K, etc., distributions within individual cells. Since this methodology does not fracture every cell on the silicon substrate, examining a particular cell with both of the imaging techniques (fluorescence and ion microscopy) is difficult. Three unsuccessful attempts were made to image the same cell with both techniques. To compare the same cell by these two imaging techniques, nearly all cells on a wafer need to be examined optically with fura-2 first and then by ion microscopy. In addition, even if the same cell is analyzed with both techniques, the sampling volume between techniques will be different (see below). Therefore, the observations on free Ca^{2+} and total Ca reported in this paper are based on sister cells maintained under identical experimental conditions.

The publication costs of this article were defrayed in part by page charge payment. This article must therefore be hereby marked "*advertisement*" in accordance with 18 U.S.C. §1734 solely to indicate this fact.

‡Present address: Department of Biochemistry, University of Massachusetts, Amherst, MA 01003.

Cell Cultures and Fura-2 Loading and Optical Imaging. Dulbecco's modified Eagle's medium (DMEM) with 10% fetal calf serum and DMEM with 10% calf serum were the cell growth media used, respectively, for NIH 3T3 fibroblast and L6 myoblast cultures. Fura-2 was loaded into the cells by adding the acetoxymethyl ester fura-2/AM (2 μM) (Molecular Probes) from a 2 mM stock dissolved in dry dimethyl sulfoxide to the culture medium and incubating the cells for 30 min at 37°C in a 5% CO_2/95% air incubator. The details of the image collection and processing system have been described elsewhere (9). Images of the free Ca^{2+} distribution within cells were produced by a method very similar to that described by Williams *et al.* (10), which has been described (11–13).

Subcellular Total Ca, K, Na, and Mg Imaging. A Cameca IMS-3f ion microscope was used for intracellular total Ca imaging. Since ion microscopy is a multielement technique, distributions of K, Na, and Mg were also studied. The ion microscope, based on secondary ion mass spectrometry, is a direct imaging mass spectrometer, which allows subcellular imaging of secondary ions sputtered from the sample surface upon primary ion beam bombardment. The visual secondary ion images reveal the elemental (total Ca, K, Na, etc.) distribution in relation to cell morphology with a spatial resolution of $\approx$0.5 μm. An O_2^+ primary ion beam with an energy of 8.0 keV was used for the study, and positive secondary ions were monitored for image detection. The primary beam current of 300 nA (spot size, $\approx$100 μm in diameter) was used with a raster of 250 $\times$ 250 μm^2. The secondary ion images of $^{40}Ca^+$, $^{24}Mg^+$, $^{39}K^+$, and $^{23}Na^+$, respectively, were recorded on Kodak Tri-X ASA 400 film using a 35-mm camera by photographing the fluorescent screen of the ion microscope. The image exposure time for K images was 1/8th sec, while times for Ca images from 3T3 and L6 cells were 85 and 120 sec, respectively.

Subcellular Total Ca Quantitation. A potassium normalization approach was used to quantitate intracellular total Ca intensities. Secondary ion mass spectrometry matrix effects have been found to be negligible between the nuclei and cytoplasm of NIH 3T3 and several other cell lines (14). This has allowed us to compute pixel-by-pixel quantitative values for intracellular total Ca in NIH 3T3 cells by normalizing the $^{40}Ca^+$ ion image to the $^{39}K^+$ ion image (quantitation for L6 myoblast cells was not undertaken for total Ca for the reasons given below). We have assumed that 3T3 cells contain 160 mM potassium (a typical number for mammalian cells) for computing quantitative values for total Ca. Except for the ion image integration time (exposure time) on photographic film, the rest of the instrumental conditions remained identical between the $^{40}Ca^+$ and $^{39}K^+$ secondary ion image recording. Linearity of the film response was established by recording a $^{28}Si^+$ ion image from an *n*-type silicon wafer (single crystal) by varying the exposure times under identical instrumental conditions. Microdensitometer film digitization was used to obtain this calibration curve (15). Both the $^{40}Ca^+$ (85-sec exposure time) and $^{39}K^+$ (1/8th-sec exposure time) ion micrographs were digitized with the microdensitometer under identical conditions. The optical density of the negative from both images was within the range of the calibration curve; hence, the images reflected the true ion counts. the $^{40}Ca^+$ ion image was then registered pixel-by-pixel with the $^{39}K^+$ image by digital image superposition with a first-order polynomial mapping function (16) to correct mass-dependent image shifting. A normalized $^{40}Ca^+/^{39}K^+$ image was obtained by dividing the registered $^{40}Ca^+$ image by the $^{39}K^+$ image. The heterogeneous microchannel plate response of the ion microscope is corrected in this approach. Seven cells were randomly selected to estimate the $^{40}Ca^+$ ion counts using the normalized $^{40}Ca^+/^{39}K^+$ image. Average relative ion counts per pixel and the total number of pixels inside the nucleus as well as inside the cytoplasm from each cell were calculated (correcting for exposure time) by using the secondary ion mass image processing system (17). These ion counts were then converted to concentration by using the K concentration of 160 mM and a relative sensitivity factor Ca/K = 0.314 for animal tissues (18). Finally, the Ca concentrations were corrected for isotopic abundances of ^{40}Ca and ^{39}K isotopes.

RESULTS

From the fura-2 fluorescence image pair of several NIH 3T3 fibroblasts (Fig. 1 *a* and *b*) is derived the free Ca^{2+} distributions of Fig. 1*c*, which are highly heterogeneous across the cells. The region of the cells corresponding to the nucleus displays Ca^{2+} levels below that of adjacent cytoplasm, while peripheral areas, particularly lamellipodia, have even lower Ca^{2+}. For the four cells in the center of the field, the free Ca^{2+} levels in the nuclei range from 75 to 150 nM with the mean $\pm$ SD for the four cells being 110 $\pm$ 30 nM. The peak cytoplasmic Ca^{2+} levels near the nuclei for these cells range from 200 to 800 nM, with a mean $\pm$ SD of 490 $\pm$ 270 nM. The ratio of cytoplasmic to nuclear free Ca^{2+} for these cells ranges from 2.7 to 5.3 with a mean $\pm$ SD of 4.3 $\pm$ 1.2. This heterogeneity within and among cells was found consistently for all 3T3 cells grown on silicon or on glass for which the intracellular organelle structure, particularly the nucleus, was visualized in unprocessed 365- or 334-nm excited fluorescence. The low-fluorescence areas in the center of the cell were identified as nuclei by transmitted light microscopy for the cells on glass coverslips (data not shown). The appearance of intracellular Ca^{2+} heterogeneities appears to be related to cell geometry—flat cells are more heterogeneous than rounded cells. This effect is likely related to the relative contributions of out-of-focus fura-2 fluorescence (see below).

The distribution of total Ca measured by ion microscopy in 3T3 cells (Fig. 1*e*) indicates a large difference between the cytoplasm and nucleus (brightness indicates relative secondary ion intensities within an image) for each cell in the field of view. At the same time, the distribution of total K in these same cells is relatively homogeneous (Fig. 1*d*). Digital quantitation of the Ca image reveals that for the seven representative cells in the field of view the total Ca levels in the nuclei range from 152 to 322 μM with the mean $\pm$ SD for the seven cells being 225 $\pm$ 43 μM. The cytoplasmic total Ca levels for these cells range from 272 to 776 μM, with a mean of 559 $\pm$ 184 μM. The ratio of cytoplasmic to nuclear total Ca for these cells ranges from 1.9 to 3.1 with a mean $\pm$ SD of 2.4 $\pm$ 0.6. On a quantitative scale, the cell nuclei are less heterogeneous than the cytoplasm for total Ca distribution (see three cells from Fig. 1*e* digitally manipulated to a quantitative total Ca scale in Fig. 1*f*).

Results somewhat similar to those for 3T3 fibroblasts are found for L6 muscle myoblast cells. Most of the L6 cells examined for free Ca^{2+} were isolated and thus were of tubular geometry; in such cells, the fura-2 fluorescence appears to be uniformly distributed within the cell (Fig. 2 *a* and *b*), while the free Ca^{2+} is only slightly heterogeneous (Fig. 2*c*), particularly in comparison with the flat fibroblast of Fig. 1. However, the pattern of heterogeneity of free Ca^{2+} within these cells is qualitatively different from the fibroblasts; levels of Ca^{2+} in the vicinity of the nucleus ($\approx$250 nM) appear somewhat higher than those in the surrounding cytoplasm ($\approx$75 nM), a result similar to that found in smooth muscle (10). Caution must be exercised in this interpretation since little intracellular structure can be defined in the unprocessed fluorescence image, and thus identification of the cytoplasmic structures contributing to the fura-2 ratio image is complicated. Ion microscopy revealed the total K and Ca distributions in confluent L6 cells (Fig. 2 *d* and *e*) to be similar to those in NIH 3T3 cells. Isolated cells showed a similar

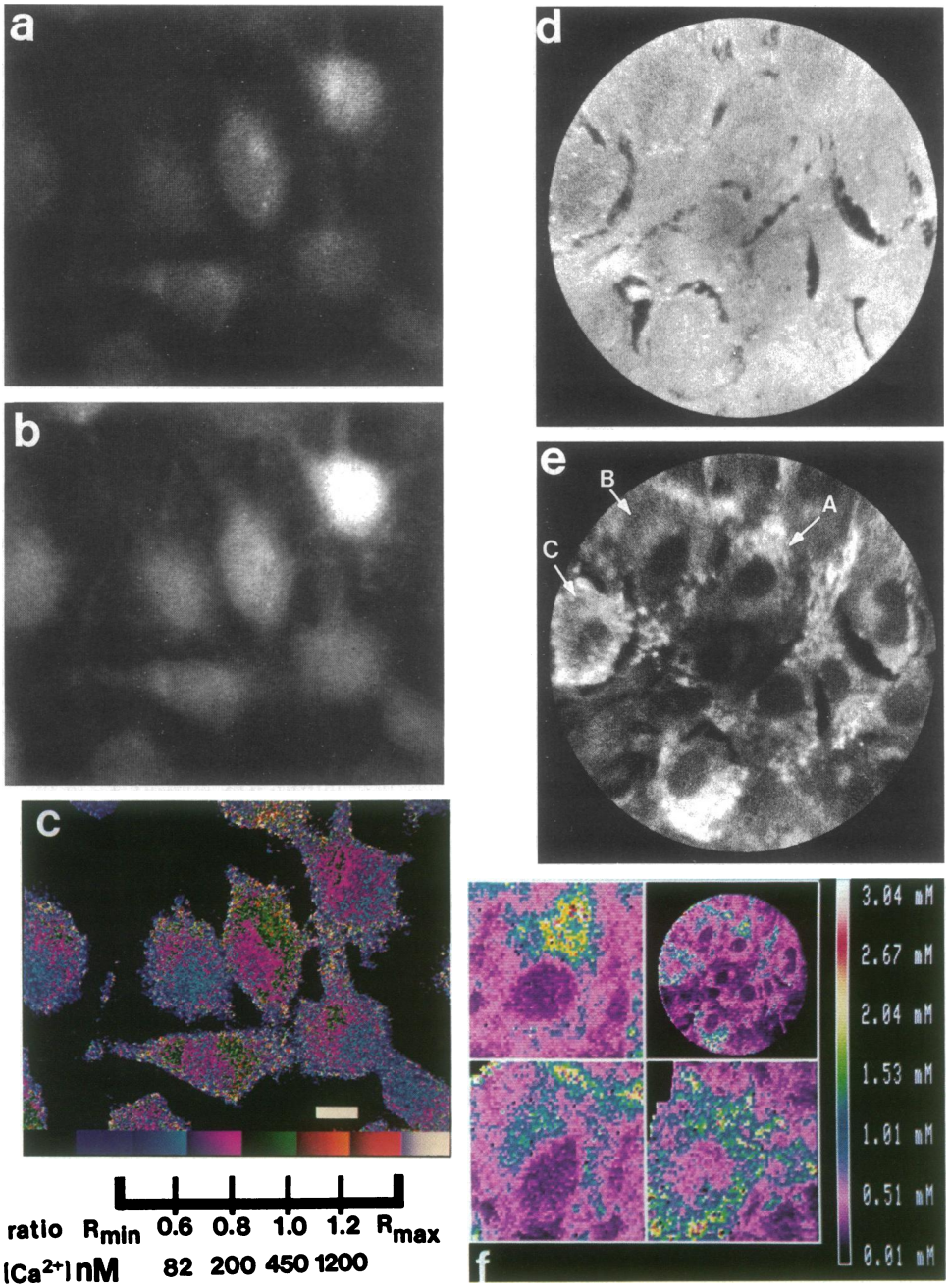

FIG. 1. Calcium distribution in NIH 3T3 fibroblasts. The free Ca^{2+} is determined from the ratio of two fura-2 fluorescence images with background subtracted; they are shown for both the numerator recorded with 334-nm excitation using a 420-nm long-pass barrier filter (*a*) and the denominator recorded with 365-nm excitation also using a 420-nm barrier (*b*). The ratio of these images gives the free Ca^{2+} distributions within the cells shown in *c*. (Bar = 10 μm.) The magnitude of the ratio and thus the Ca^{2+} levels in the cells are shown in pseudocolor, the calibration of which is given below the ratio image. Ion microscopic images of potassium ($^{39}K^+$) and calcium ($^{40}Ca^+$) reveal the intracellular distribution of total K (*d*) and Ca (*e*), respectively, for a group of confluent cells that have all been freeze-fractured and freeze-dried. The dark regions in the potassium image represent extracellular spaces between cells. Cells A, B, and C are shown on a quantitative scale in *f*. For ion microscope images, image exposure times are as follows: $^{39}K^+$, 1/8th sec; $^{40}Ca^+$, 85 sec. Image field of view, 150 μm in diameter. (*f*) Intracellular total Ca distribution on a quantitative scale. The image on the top right square is the $^{40}Ca^+/^{39}K^+$ normalized image. Three individual cells are magnified to show the quantitative distribution of total Ca. Cells A, B, and C of *e* are in the top left, bottom left, and bottom right square, respectively, of this image. The area of a small square is 35 μm^2.

pattern. Since we are not confident of free Ca^{2+} quantitation in L6 cells, total Ca quantitative numbers were not computed for comparisons.

The loading of fura-2 did not alter the subcellular total Ca distribution in either cell line (ion images not shown). In addition, the subcellular distributions of total K, Na, and Mg revealed by ion microscopy also remained comparable between fura-2-loaded and untreated controls. These observations, however, are qualitative in nature.

DISCUSSION

To quantitatively compare fura-2 images of the free Ca^{2+} distribution in a cell with ion microscope images of total Ca in the same cells or a sister cell, one must consider the differences in the mode of imaging for the two techniques. Standard fluorescence microscopy, even with a high numerical aperture objective lens, produces an imperfect image of the plane of the specimen, which is in focus because of the relatively efficient capture of light emanating from out-of-focus planes in the specimen. Note that for a relatively round 3T3 cell in Fig. 1 *a–c*, for which little intracellular structure is seen in the unprocessed fluorescence images (the cell on the top right corner), the free Ca^{2+} distribution appears more uniform than for the flatter cells. In contrast, ion microscopic images for total Ca are based on surface sputtering and thus represent a horizontal section through the cells. For the total Ca images in Figs. 1*e* and 2*e*, integration times correspond to 0.2- to 0.3-μm-thick sections of the cells.

To interpret these results, the potential artifacts of both techniques must also be considered. The sandwich-fracture methodology for ion microscopy used in the present study depends entirely on reliable cryotechniques for sample fixation and excludes steps that are susceptible to contamination (4). The reliability of this methodology has been confirmed by successfully imaging Na^+/K^+ transport after inhibition of the sodium pump with ouabain in several cell lines (19). The potential ion microscopic artifacts of the $^{39}KH^+$ mass interference with $^{40}Ca^+$, differential sputtering between the cell nucleus and cytoplasm, and local matrix

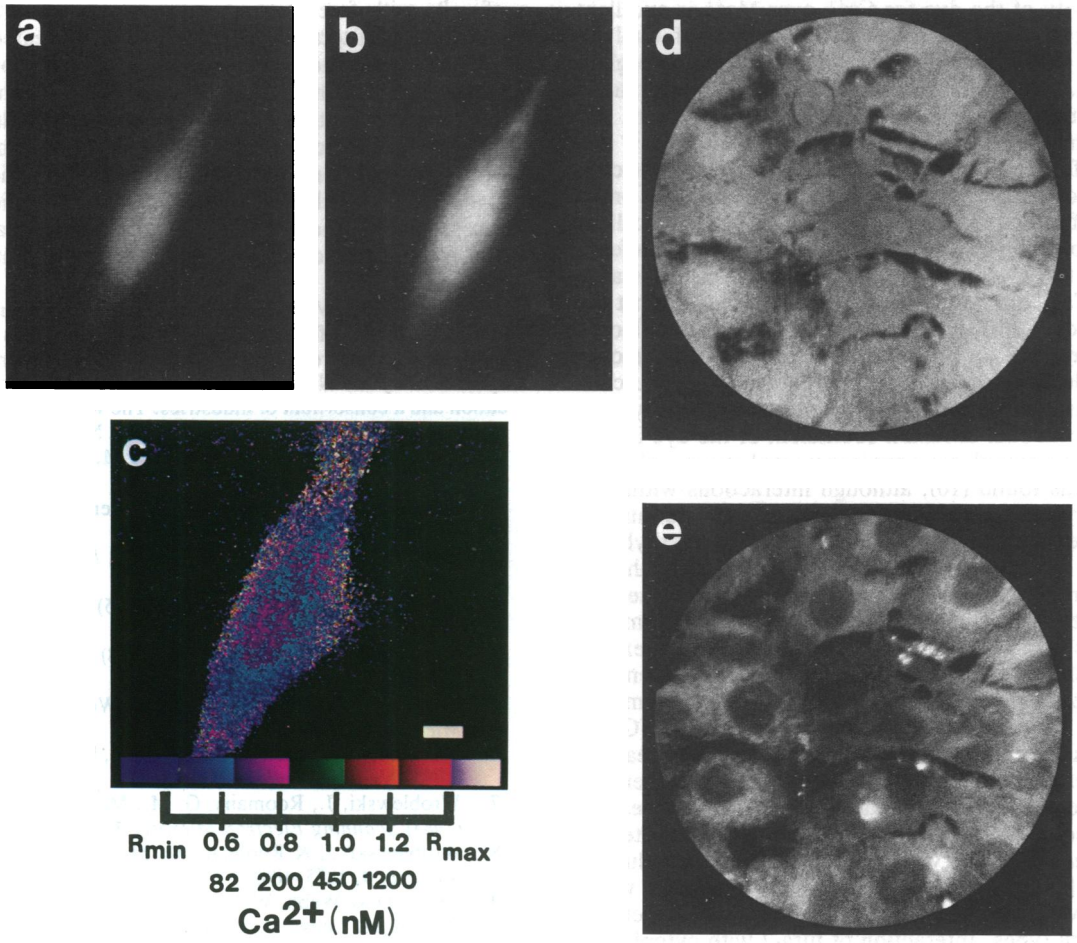

FIG. 2. Calcium distribution in L6 myoblast cells. The background-subtracted fluorescence images for the numerator (*a*) and denominator (*b*) images that yield the Ca^{2+} ratio images (*c*) were collected as described in the text and legend to Fig. 1. The very dim region of the cell not easily visible in *a* and *b* produced the noisy Ca^{2+} "halo" in *c*. (Bar = 10 μm.) (*d* and *e*) Ion microscope images of total K and Ca, respectively, for the field of the same kind of cells. For ion microscope images, image exposure times are as follows: $^{39}K^+$, 1/8th sec; $^{40}Ca^+$, 120 sec. Image field of view, 150 μm in diameter.

effect variations were found to be insignificant in 3T3 cells and several other cell lines (14). In addition, sandwich-fractured freeze-dried cells examined by scanning electron microscopy revealed structural preservation far beyond the spatial resolution of the ion microscope (20). In the potassium normalization approach of total Ca quantitation, we assumed a value for intracellular potassium concentration of 160 mM. Changing this estimate by ±10 mM alters the calculated Ca concentration by only 6.25%.

Little is known about the possible artifacts of free Ca^{2+} measurements using fura-2 fluorescence since the dye and the digital imaging technology are recent innovations (1). We (D.G. and P. Millard, unpublished observations) have from time to time noticed fura-2-loaded rat basophilic leukemia cells dividing normally during time-lapse imaging of free Ca^{2+}, which suggests the absence of severe toxic effects of the dye and exposure to ultraviolet light under our conditions. Others have also reported similar observations (21).

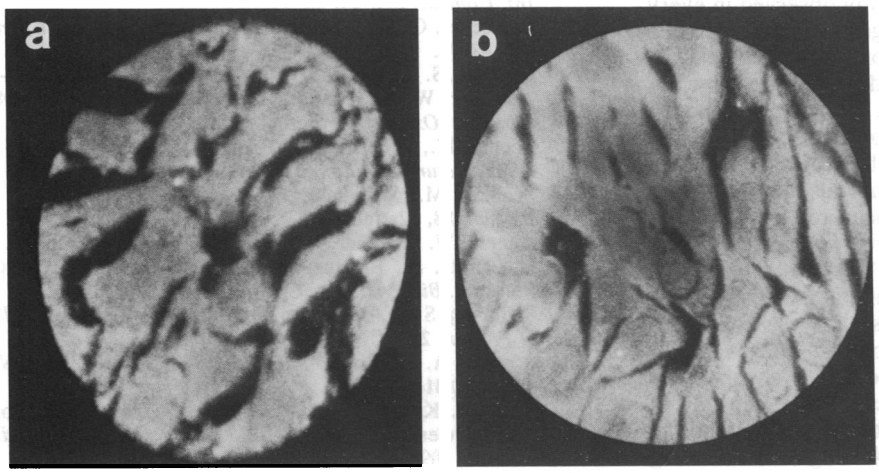

FIG. 3. Ion microscopic images of total cellular magnesium in NIH 3T3 cells (*a*) and L6 cells (*b*). Individual cells are separated by dark extracellular spaces. Image exposure time, 60 sec. Image field of view, 150 μm in diameter.

The selectivity of the dye for Ca^{2+} over Mg^{2+} is excellent, ≈25,000:1 (1). In any case, the distribution of total Mg revealed by ion microscopy seems homogeneous throughout the cell (Fig. 3); thus, it is unlikely to introduce an artifact in the localization of free Ca^{2+} in fura-2 measurements. The ability of the free fura-2 indicator dye to bind Ca^{2+} and thereby buffer temporal or spatial gradients within the cytoplasm is a potential source of artifact, which depends on the relative buffering capacity of fura-2 at typical intracellular concentrations of ≈100 μM relative to the intrinsic buffering capacity of the cytoplasm. Measured [Ca^{2+}] levels near or above the Ca^{2+} binding constant of fura-2 indicate that this artifact is not significant. Alterations of the fura-2 fluorescence spectrum or Ca^{2+} binding constant due to interaction with subcellular components is another potential source of artifact. This point has been indirectly addressed by comparing the rotational diffusion coefficient of the dye in both the nuclear and cytoplasmic environments between which no difference was found (10), although interactions within cytoplasmic organelles were not studied. Incomplete intracellular esterase cleavage of the fura-2 tetraacetoxymethyl ester has recently been shown to complicate the ratio method of [Ca^{2+}] determination (22). We have not attempted to measure the degree to which complete cleavage of acetoxymethyl ester groups occurs in 3T3 and L6 cells under our experimental conditions. The contribution of the fluorescence of nonhydrolyzed or incompletely hydrolyzed acetoxymethyl ester tends to depress the values of measured [Ca^{2+}]. However, as the excitation spectrum of some of the reaction intermediates peaks at 380 nm (22) and we use 365 rather than 380 nm as the denominator excitation wavelength, we expect a lesser effect on [Ca^{2+}] calibration than that reported by Scanlon *et al.* (22). This view is supported by the values of intracellular [Ca^{2+}] determined by our measurements, which are at or above the typical values measured by other methods in various cell types. Interaction of fura-2 with cytoplasmic organelles has been noted in a few cell lines (23–25). In our case, the dye stained the cells diffusely in both cell lines (see Figs. 1 and 2) as opposed to the specific localization as shown for mitochondria in bovine aortic endothelial cells (25). Interaction of fura-2 with cytoplasmic organelles and an understanding of such an interaction in affecting the cytosolic free Ca^{2+} measurements remains a challenging area of research. On the other hand, in the absence of a known intranuclear membrane structure, fura-2 should reveal the "true intranuclear free Ca^{2+}" concentrations. It is interesting to note that for both free and total calcium measurements, our data reveal a lesser degree of heterogeneity in the cell nucleus.

Individual cells differed in both free and total Ca, indicating the dynamic state of this ion. In both cell lines, the disposition of total Ca indicates that stores of calcium are greater in the cytoplasm than in the nucleus. A sharp drop in the total Ca from cell cytoplasm to the nuclear region observed in every cell in the ion microscopic images suggests the presence of a Ca storage organelle in close apposition to the nucleus. The endoplasmic reticulum is a good candidate, and the same has been shown to be a Ca storage site (26). Mitochondria and the newly discovered cytoplasmic "calciosome" organelle (27) are other Ca interacting sites in the cell cytoplasm. Calcium binding proteins such as calmodulin may also play a role in free Ca^{2+} homeostasis. The total Ca measured by ion microscopy contains contributions from free, sequestered, and bound calcium. Our measurements on 3T3 cells indicate that total Ca values are ≈3 orders of magnitude greater in either nuclear or cytoplasmic compartments than the free Ca^{2+} values found with fura-2; therefore, total Ca images of 3T3 cells represent bound and sequestered Ca to a very good approximation. This result also implies that the capacity of cells to buffer Ca^{2+} is quite high in both the nucleus and the cytoplasm, a result that agrees with our finding that the loading of cells with free Ca^{2+} chelator fura-2 did not modify the distribution of total Ca as compared to untreated controls.

The present study demonstrates a powerful combination of two imaging techniques and provides a methodology for studying distribution of free and total intracellular calcium under physiological, pathological, and toxicological conditions. In addition, the ability of the ion microscope to measure the distribution of other elemental species allows the assessment of whole cell viability and subcellular activity as well as enhances confidence in the measurement of calcium.

We thank Watt W. Webb for support and stimulating discussions and James Willard for culturing cells. This work was supported (in part) by a grant from Cornell Biotechnology Program, which is sponsored by the New York State Science and Technology Foundation and a consortium of industries. The work was also supported by the National Institutes of Health (Grant NIH GM33028 to W. W. Webb and Grant NIH GM24314 to G.H.M.).

1. Grynkiewicz, G., Poenie, M. & Tsien, R. Y. (1985) *J. Biol. Chem.* **260,** 3440–3450.
2. Castaing, R. & Slodzian, G. (1962) *J. Microsc. (Paris)* **1,** 395–410.
3. Morrison, G. H. & Slodzian, G. (1975) *Anal. Chem.* **47,** 932A–943A.
4. Chandra, S. & Morrison, G. H. (1988) *Methods Enzymol.* **158,** 157–179.
5. Chandra, S., Morrison, G. H. & Wolcott, C. C. (1986) *J. Microsc. (Oxford)* **144,** 15–37.
6. Nakache, M., Schreiber, A. B., Gaub, H. & McConnell, H. M. (1985) *Nature (London)* **317,** 75–77.
7. Wroblewski, J., Roomans, G. M., Madsen, K. & Friberg, U. (1983) *Scanning Electron Microsc.* **2,** 777–784.
8. Wroblewski, J. & Roomans, G. M. (1984) *Scanning Electron Microsc.* **4,** 1875–1882.
9. Gross, D. & Webb, W. W. (1988) in *Spectroscopic Membrane Probes*, ed. Loew, L. M. (CRC, Boca Raton, FL), Vol. 2, pp. 19–45.
10. Williams, D. A., Fogarty, K. E., Tsien, R. Y. & Fay, F. S. (1985) *Nature (London)* **318,** 558–561.
11. Millard, P. J., Gross, D., Webb, W. W. & Fewtrell, C. (1988) *Proc. Natl. Acad. Sci. USA* **85,** 1854–1858.
12. Gonzalez, F. A., Heppel, L. A., Gross, D. J., Webb, W. W. & Parries, G. (1988) *Biochem. Biophys. Res. Commun.* **151,** 1205–1212.
13. Gonzalez, F. A., Gross, D. J., Heppel, L. A. & Webb, W. W. (1988) *J. Cell. Physiol.* **135,** 269–276.
14. Chandra, S., Ausserer, W. A. & Morrison, G. H. (1987) *J. Microsc. (Oxford)* **148,** 223–239.
15. Ling, Y.-C., Bernius, M. T. & Morrison, G. H. (1986) *Instruction Manual for IMGSCN* (Cornell Univ., Ithaca, NY), Material Science Rep. 5921.
16. Turner, L. K., Ling, Y.-C., Bernius, M. T. & Morrison, G. H. (1987) *Anal. Chem.* **59,** 2463–2468.
17. Ling, Y.-C., Bernius, M. T. & Morrison, G. H. (1987) *J. Chem. Inf. Comput. Sci.* **24,** 86–95.
18. Ramseyer, G. O. & Morrison, G. H. (1983) *Anal. Chem.* **55,** 1963–1970.
19. Chandra, S. & Morrison, G. H. (1985) *Science* **228,** 1543–1544.
20. Ausserer, W. A., Chandra, S. & Morrison, G. H. (1989) *J. Microsc. (Oxford)*, in press.
21. Poenie, M., Alderton, J., Tsien, R. Y. & Steinhardt, R. A. (1985) *Nature (London)* **315,** 147–149.
22. Scanlon, M., Williams, D. A. & Fay, F. S. (1986) *J. Gen. Physiol.* **88,** 52a (abstr.).
23. Almers, W. & Neher, E. (1985) *FEBS Lett.* **192,** 13–18.
24. Highsmith, S., Bloebaum, P. & Snowdowne, K. W. (1986) *Biochem. Biophys. Res. Commun.* **138,** 1153–1162.
25. Steinberg, S. F., Bilezikian, J. P. & Al-Awqati, Q. (1987) *Am. J. Physiol.* **253,** C744–C747.
26. Somlyo, A. P., Bond, M. & Somlyo, A. V. (1985) *Nature (London)* **314,** 622–625.
27. Volpe, P., Krause, K.-H., Hashimoto, S., Zorzato, F., Pozzan, T., Meldolesi, J. & Lew, D. P. (1988) *Proc. Natl. Acad. Sci. USA* **85,** 1091–1095.